Critical transition for colliding swarms

Jason Hindes[1], **Victoria Edwards**[1,2]**, M. Ani Hsieh**[2] **and Ira B. Schwartz**[1]

[1]U.S. Naval Research Laboratory, Washington, DC 20375, USA
[2]Mechanical Engineering and Applied Mechanics, University of Pennsylvania, Philadelphia, Pennsylvania 19104, USA

E-mail: `jason.hindes@nrl.navy.mil`

Abstract. Swarming patterns that emerge from the interaction of many mobile agents are a subject of great interest in fields ranging from biology to physics and robotics. In some application areas, multiple swarms effectively interact and collide, producing complex spatiotemporal patterns. Recent studies have begun to address swarm-on-swarm dynamics, and in particular the scattering of two large, colliding swarms with nonlinear interactions. To build on early numerical insights, we develop a mean-field approach that can be used to predict the parameters under which colliding swarms are expected to form a milling state. Our analytical method relies on the assumption that, upon collision, two swarms oscillate near a limit-cycle, where each swarm rotates around the other while maintaining an approximately constant and uniform density. Using this approach we are able to predict the critical swarm-on-swarm interaction coupling, below which two colliding swarms merely scatter, for near head-on collisions as a function of control parameters. We show that the critical coupling corresponds to a saddle-node bifurcation of a stable limit cycle in the uniform, constant density approximation. Our results are tested and found to agree with large multi-agent simulations.

1 Introduction

Swarming occurs when spatiotemporal patterns and behaviors emerge from the interaction of large numbers of coupled mobile systems, typically with fairly limited capabilities and local dynamics. Examples have been discovered in nature over many spatiotemporal scales from colonies of bacteria, to swarms of insects[1, 2, 3, 4], flocks of birds [5, 6, 7], schools of fish[8, 9], crowds of people[10], and active-matter systems more generally[11]. Understanding the principles behind swarming patterns and describing how they emerge from simple models has been the subject of significant work in physics, applied mathematics, and engineering sciences [12, 13, 14, 15, 16, 17, 18, 19, 20, 21, 22, 23, 24]. Parallel with this work, and because of the robustness, scalability, and collective-problem solving capabilities of natural swarms, much research has focused on designing and building swarms of mobile robots with a large and ever expanding number of platforms, as well as virtual and physical interaction

mechanisms[11, 25, 26, 27, 28]. Applications for such systems range from exploration[26], mapping[29], resource allocation [30, 31, 32], and swarms for defense [33, 34, 35]

Since the overall cost of robotic systems has decreased significantly in recent years, it has become possible to use artificial swarms in the real world [36, 37, 27, 26]. This introduces the possibility of having multiple swarms occupying the same physical space, resulting in mutual interactions and perturbations of one another's dynamics[38]. As the potential for such swarm-on-swarm interactions increases, an understanding of how multiple swarms collide and merge becomes necessary.

Though much is known about the behaviors and stability of single isolated swarms with physically-inspired, nonlinear interactions[39, 40, 41, 42, 43], much less is known about the intersecting dynamics of multiple such swarms, even in the case where one swarm is a single particle, as in predator–prey modeling[44]. Recent numerical studies have shown that when two flocking swarms collide, the resulting dynamics typically appear as a merging of the swarms into a single flock, milling as one uniform swarm, or scattering into separate composite flocks moving in different directions[45, 46, 38]. Though interesting, a more detailed analytical understanding of how and when these behaviors occur is needed, especially when designing robotic swarm experiments, and controlling their outcomes.

To make progress, we consider a generic system of mobile agents moving under the influence of self-propulsion, friction, and pairwise interaction forces. In the absence of interactions, each swarmer tends to a fixed speed, which balances its self-propulsion and friction but has no preferred direction[47]. A simple model that captures the basic physics is

$$\ddot{\mathbf{r}}_i = \left[\alpha_i - \beta|\dot{\mathbf{r}}_i|^2\right]\dot{\mathbf{r}}_i - \lambda_i \sum_{j \neq i} \partial_{\mathbf{r}_i} U(|\mathbf{r}_j - \mathbf{r}_i|) \tag{1}$$

where $\mathbf{r}_i$ is the position-vector for the ith agent in two spatial dimensions, α_i is a self-propulsion constant, β is a friction constant, and λ_i is a coupling constant[39, 40, 41, 42, 43]. The total number of swarming agents is N. Beyond providing a basis for theoretical insights, Eq.(1) has been implemented in experiments with several robotics platforms including autonomous ground, surface, and aerial vehicles[48, 49, 50].

An example interaction potential that we consider in detail is the Morse potential,

$$U(r) = Ce^{-r/l} - e^{-r} \tag{2}$$

– a common model for soft-core interactions with local repulsion and attraction ranges, scaled as l and 1, respectively[42, 51]. In the following, we assume that two interacting swarms are subject to the same underlying physics, Eqs.(1-2), but with different initial conditions and potentially different control parameters. In particular, we assume that within each swarm the parameters are homogeneous, e.g., $\alpha_i \in \{\alpha^{(1)}, \alpha^{(2)}\}$ and $\lambda_i \in \{\lambda^{(1)}, \lambda^{(2)}\}$, where the superscripts (1) and (2) denote the first and second swarms, respectively. The assumption that the two swarms satisfy the same basic physics makes sense if the swarms are composed of similar agents, and should be a reasonable, baseline assumption for biological and active-matter swarm collisions.
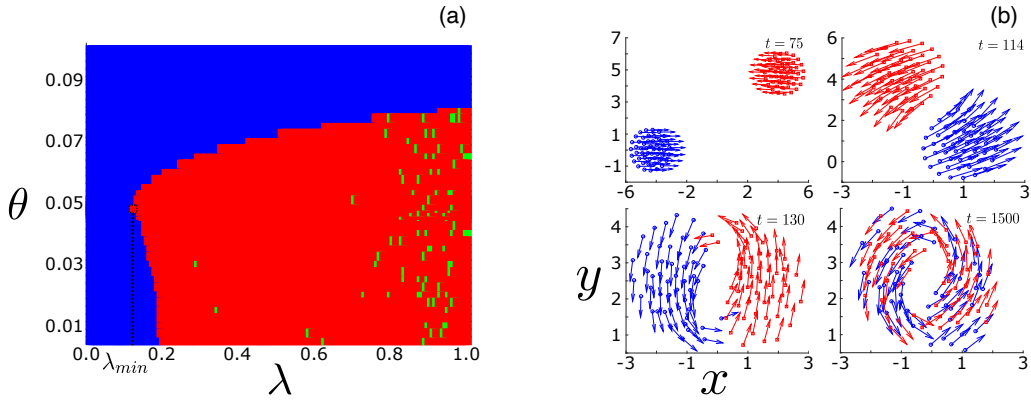
2 Collision of two flocking swarms

As in [45, 46], we are interested in the collision of two flocking swarms composed of approximately equal numbers of agents (in the absence of any communication delay). The swarms are each prepared in a flocking state with initial velocities and positions that are a large distance D from the collision region, such that $\mathbf{r}_i = \mathbf{d}_i^{(1)} - D\,\hat{\mathbf{x}}$ and $\dot{\mathbf{r}}_i = \sqrt{\alpha^{(1)}/\beta}\,\hat{\mathbf{x}}$ if $i \in (1)$, and $\mathbf{r}_i = \mathbf{d}_i^{(2)} + D\sqrt{\alpha^{(2)}/\alpha^{(1)}}(\cos(\theta)\hat{\mathbf{x}} + \sin(\theta)\hat{\mathbf{y}})$ and $\dot{\mathbf{r}}_i = \sqrt{\alpha^{(2)}/\beta}(-\cos(\theta)\hat{\mathbf{x}} + \sin(\theta)\hat{\mathbf{y}})$ if $i \in (2)$. The internal flocking coordinates, $\mathbf{d}_i^{(1)}$ and $\mathbf{d}_i^{(2)}$, represent local minimum energy configurations (MECs), $-\partial_{\mathbf{d}_i} U(|\mathbf{d}_j - \mathbf{d}_i|) = \mathbf{0}_i\ \forall i$ [52]. Before colliding, the swarms are assumed to be far apart, $D \gg 1$, with a collision angle θ. Note that given this setup, the net force on every agent is initially zero (a consequence of the MEC and the finite-range of interactions), and the swarms collide near the origin.

Qualitatively, for relatively small θ the two flocks typically scatter or mill depending on the coupling strength and relative velocities. In the former the swarms leave the collision region in separate flocking states with perturbed velocities. In the latter they form a milling state, and circulate around a stationary center of mass. Figure 1(a) gives an example scattering diagram for the collision of symmetric flocks with equal parameters. The two final swarm states are specified with blue and red for scattering and milling, respectively; the green portions indicate the formation of a combined flocking state, which is comparatively infrequent for the parameters shown. For small θ we can see that the combined milling state (MS) appears for couplings above a certain value λ_{min}– the smallest coupling needed to form a MS. This *critical coupling* will be a primary focus in what follows.

In order to visualize collisions that result in milling states, we show four time-snapshots in Figure 1(b) when $\lambda = \lambda_{min}$. Agents in the two swarms are drawn with different colors, and their velocities shown with arrows. In the first snapshot (upper left), the swarms approach collision with configurations and velocities identical to those specified in the first paragraph of this section– namely, the MEC with constant velocity. In the second snapshot (upper right) the swarms rotate around each other with a constantly changing heading, roughly uniform velocity distribution, and a configuration approximately equal to the MEC. Over time each swarm's density elongates in the direction of rotation (third snapshot, lower left), as the velocity distribution becomes less homogeneous. Finally, on long times scales the two swarms blend into one and form a MS with agents from each uniformly distributed across the whole. This qualitative sequence holds more generally within the red region of Fig. 1(a).

In order to predict the critical coupling, λ_{min}, our approach is to find an analytical description of the collision dynamics that is applicable for the first two snapshots in Figure 1(b), where two approximately MEC flocks approach, and then rotate around a common center. Our conjecture is that if such rotations are approximately stable, then a MS occurs upon collision (and visa versa). Though we will analyze two-flock collisions in this way assuming Morse-potential interactions, Eq.(2), our method should be applicable

Figure 1. Collision of two symmetric flocks. (a) Scattering digram indicating the final, aggregate swarm state as a function of the collision angle and coupling: scattering (blue), milling (red), and single-flock (green). The critical coupling is specified with a dashed vertical line, and separates the scattering and milling regions. (b) Four time-snapshots for $\lambda = \lambda_{min}$ showing each swarm with different colors: red squares and blue circles. Velocities are drawn with arrows. Swarm parameters are $\alpha = 1$, $\beta = 5$, $C = 10/9$, $l = 0.75$, and $N = 100$.

to a broad range of second-order dynamical swarms given position-dependent, nonlinear interactions with finite attractive and repulsive length scales.

2.1 Uniform constant density approximation

First, we would like to find a low-dimensional approximation for the flocking state dynamics. A clue comes from Figure 2(a), which plots the fraction of nodes at a given distance r from the center of mass (CM) of a single moving flock for different values of the repulsion strength, C. We can see that the radial distribution is approximately *linear* in r. Moreover, since the potential is radial, we expect the steady-state angular distribution to be uniform; the inlet panel shows an example flocking state with such a spatial distribution of agents. Together, these imply a roughly uniform density in the flocking state, $\rho = N/\pi R^2$, where R is the maximum radius. Given the uniform-density assumption, the predicted fraction of agents at a given r is $f(r) = 2r\Delta r/R^2$, where Δr is the bin-size used to plot the distribution. This prediction is drawn with lines for comparison in Figure 2(a).

Assuming a uniform density, we can describe a flock in general by its CM-dynamics and the boundary radius, R. In particular, every agent, including those on the boundary, move with constant speed, $\sqrt{\alpha/\beta}$, where α is the self-propulsion constant for the flock. A self-consistent formula can be derived for R, and used to compute it, by satisfying force-balance on the boundary. For example, consider an agent with $\mathbf{d}_i = R\,\hat{\mathbf{x}}$. The
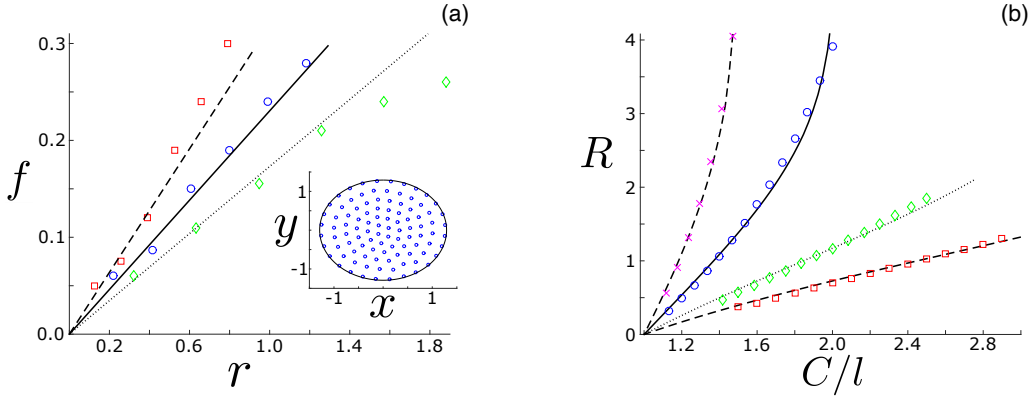
Figure 2. Uniform constant density approximation for flocking states (UCDA). (a) fraction of agents a distance r from the center of mass for $C = 1.0$ (red-squares), 1.1 (blue-circles), 1.25 (green-diamonds) when $l = 0.75$, where C is the repulsive-force strength with length-scale l. The dashed, solid, and dotted lines indicate UCDA predictions from solving Eq.(3). The inlet panel shows an example flocking state with the UCDA boundary drawn in black for $C = 1.1$. (b) Flocking state boundary, $R = \max\{r\}$, from simulations: ($l = 0.85$, magenta-xs), ($l = 0.75$, blue-circles), ($l = 0.60$, green-diamonds) and ($l = 0.50$, red-squares) compared to UCDA predictions shown with lines near each series. Other swarm parameters are $\alpha = 1$, $\beta = 5$, $\lambda = 2$, and $N = 100$.

x-component of the interaction force must be zero,

$$0 = \int_0^{2\pi}\int_0^1 \left(\frac{C}{l}e^{-\frac{R}{l}\sqrt{1+u^2-2u\cos\phi}} - e^{-\sqrt{1+u^2-2u\cos\phi}}\right)$$
$$\cdot \frac{u\cos\phi - 1}{\sqrt{1 + u^2 - 2u\cos\phi}} \cdot u\,du\,d\phi\,, \tag{3}$$

where $u \equiv r/R$. Note that the y-component of the force is trivially zero due to the uniform-angular distribution of agents. Comparisons between simulations and numerical solutions to Eq.(3) are shown in Fig.2(b) for a range of control parameters, and indicate good agreement.

Next, we can approximate the initial collision dynamics of two flocks by assuming that the uniform density configuration is maintained within each flock, with a boundary given by Eq.(3). Namely, the mean-field collision-model that we will analyze below is of two interacting, constant-density disks composed of self-propelled particles. Consider an agent positioned at the CM of each swarm, $\mathbf{r}^{(1)}(t)$ and $\mathbf{r}^{(2)}(t)$. Such agents feel self-propulsion, friction, and interaction forces, just as in Eq.(1). However, the non-zero contribution for the latter only comes from the *other flock*, since the interaction force from its own cancels, e.g., due to the MEC assumption. Moreover, the interaction force from the opposing flock is felt gradually as the two swarms approach, because of the finite-range interactions and the initially large separation between the flocks. To find the non-zero contribution, we simply need to integrate the interaction force over a constant-density disk of radius R, centered on the opposing swarm's CM. If we assume

that the two swarms are roughly equally sized, each with $N/2$ agents, the CM-dynamics become

$$\ddot{\mathbf{r}}^{(1)} = \left[\alpha^{(1)} - \beta|\dot{\mathbf{r}}^{(1)}|^2\right]\dot{\mathbf{r}}^{(1)} - \frac{\lambda^{(1)}N}{2}\boldsymbol{\mathcal{E}}(\mathbf{r}^{(2)}, \mathbf{r}^{(1)}; R) \tag{4a}$$

$$\ddot{\mathbf{r}}^{(2)} = \left[\alpha^{(2)} - \beta|\dot{\mathbf{r}}^{(2)}|^2\right]\dot{\mathbf{r}}^{(2)} - \frac{\lambda^{(2)}N}{2}\boldsymbol{\mathcal{E}}(\mathbf{r}^{(1)}, \mathbf{r}^{(2)}; R) \tag{4b}$$

$$\boldsymbol{\mathcal{E}}(\mathbf{r}^{(2)}, \mathbf{r}^{(1)}; R) = \int_0^{2\pi}\int_0^R \frac{\mathbf{r}^{(2)} + \mathbf{d} - \mathbf{r}^{(1)}}{|\mathbf{r}^{(2)} + \mathbf{d} - \mathbf{r}^{(1)}|} \cdot \frac{r\,dr\,d\phi}{\pi R^2}$$
$$\cdot \left(\frac{C}{l}e^{-|\mathbf{r}^{(2)}+\mathbf{d}-\mathbf{r}^{(1)}|/l} - e^{-|\mathbf{r}^{(2)}+\mathbf{d}-\mathbf{r}^{(1)}|}\right) \tag{4c}$$

$$\mathbf{d} = r\cos\phi\,\hat{\mathbf{x}} + r\sin\phi\,\hat{\mathbf{y}}, \tag{4d}$$

where $\mathbf{d}$ is an internal-coordinate inside the constant-density disk centered on the opposing swarm's CM. Equations (3-4d) constitute the mean-field dynamical system that we call the uniform constant density approximation (UCDA). The integrals in Eq.(4c) can be evaluated using e.g., trapezoid rule with 100 discretization points. Our next step is to study stable oscillations of $\mathbf{r}^{(1)}(t)$ and $\mathbf{r}^{(2)}(t)$ in the UCDA and compare to swarm collision dynamics.
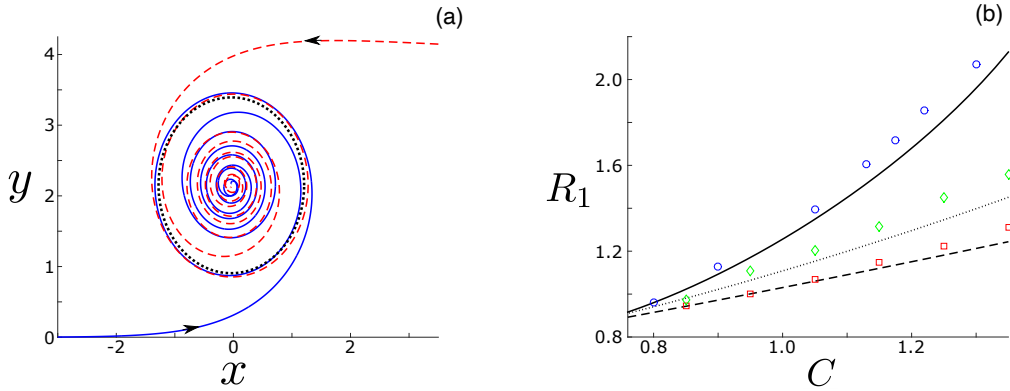
Figure 3. Collision dynamics resulting in milling. (a) Center-of-mass trajectories for two colliding swarms when $\lambda = \lambda_{min}$, shown with solid-blue and dashed-red lines. Arrows give the direction of motion. The dashed-black line indicates the bifurcating limit cycle in the uniform constant density approximation. Other swarm parameters are $\alpha = 1$, $\beta = 5$, $l = 0.75$, $N = 100$, and $C = 1.0$. (b) Maximum x-coordinate reached by the center of mass of the rightward moving (blue) flock when $\lambda = \lambda_{min}$. Simulation results are shown with blue circles for $l = 0.75$, green diamonds for $l = 0.6$, and red squares for $l = 0.5$. Limit-cycle predictions from Eqs.(5a-5d) and Eq.(6) are drawn with lines near each series. Other swarm parameters are $\alpha = 1$, $\beta = 5$, and $N = 200$.

2.2   Stable oscillations

Stable oscillations in the UCDA come in the form of circular-orbit limit cycles where both flocks oscillate around a common center with the same frequency, a fixed phase

difference, and different amplitudes in general. We can compute the parameters for such limit cycles by substituting the ansatz $\mathbf{r}^{(1)}(t) = R_1\cos(\omega t)\hat{\mathbf{x}} + R_1\sin(\omega t)\hat{\mathbf{y}}$ and $\mathbf{r}^{(2)}(t) = R_2\cos(\omega t + \gamma)\hat{\mathbf{x}} + R_2\sin(\omega t + \gamma)\hat{\mathbf{y}}$ into Eqs.(4a-4d). The result is the following four root equations satisfying $F_i = 0$ for $i \in \{1, 2, 3, 4\}$:

$$F_1 = -R_1\omega^2 + \frac{\lambda^{(1)}N}{2}\mathcal{E}_x \tag{5a}$$

$$F_2 = -R_1\omega\left[\alpha^{(1)} - \beta R_1^2\omega^2\right] + \frac{\lambda^{(1)}N}{2}\mathcal{E}_y \tag{5b}$$

$$F_3 = -R_2\omega\sin\gamma\left[\alpha^{(2)} - \beta R_2^2\omega^2\right] + R_2\omega^2\cos\gamma + \frac{\lambda^{(2)}N}{2}\mathcal{E}_x \tag{5c}$$

$$F_4 = R_2\omega\cos\gamma\left[\alpha^{(2)} - \beta R_2^2\omega^2\right] + R_2\omega^2\sin\gamma + \frac{\lambda^{(2)}N}{2}\mathcal{E}_y \tag{5d}$$

with

$$\mathcal{E}_x = \int_0^{2\pi}\int_0^R \frac{R_2\cos\gamma + r\cos\phi - R_1}{d} \cdot \left(\frac{C}{l}e^{-d/l} - e^{-d}\right)$$
$$\cdot \frac{rdrd\phi}{\pi R^2} \tag{5e}$$

$$\mathcal{E}_y = \int_0^{2\pi}\int_0^R \frac{R_2\sin\gamma + r\sin\phi}{d} \cdot \left(\frac{C}{l}e^{-d/l} - e^{-d}\right)$$
$$\cdot \frac{rdrd\phi}{\pi R^2} \tag{5f}$$

$$d = \sqrt{(R_2\cos\gamma + r\cos\phi - R_1)^2 + (R_2\sin\gamma + r\sin\phi)^2}. \tag{5g}$$

Solutions to Eqs.(5a-5d) for $\boldsymbol{L} \equiv [R_1, R_2, \gamma, \omega]$ can be shown to exactly match limit cycles within the UCDA; more importantly, they agree with the transient oscillations for collisions in the full system, Eqs.(1-2). For example, Fig.3(a) shows CM-trajectories in red and blue for two colliding swarms when $\lambda = \lambda_{min}$. We can see that the trajectories approach the UCDA limit-cycle, shown with a black-dashed line, before slowly decaying into the origin. Using this picture as a basis, the maximum rotation radius during collisions can be compared directly to limit-cycle radii predictions from Eqs.(5a-5g). In Fig.3(b) we plot such a comparison using the maximum horizontal distance reached by the CM of the rightward moving flock (as a proxy for the collision radius). Mean-field predictions and simulations quantitatively agree fairly well over a broad range of parameter values. Qualitatively, as the repulsive-force constant C increases, the two swarms oscillate at larger distances from each other upon collision, particularly for larger values of the repulsion scale, l. This increase in rotation distance, R_1, is accompanied by a decrease in rotation frequency, $\omega \sim R_1^{-1}$.

Next, we can consider stability. When control parameters are changed (one at a time), stable limit cycles satisfying Eqs.(5a-5g) disappear generically through *saddle-node bifurcations* (SNs). As stated previously in Sec.2, a post-collision MS in the full system Eqs.(1-2) is not expected to form unless stable limit-cycles exist, and hence, λ_{min} can be approximated by the SN value in the UCDA. We can find a general condition to

determine λ_{min} at the SN through the following. Using the defined vector components $\boldsymbol{F}$ specified in Eqs.(5a-5d), we compute the derivatives of $\mathbf{F}$ with respect to the limit-cycle parameters, $\mathbf{L}$. Finally, at the SN the Jacobian matrix $\underline{J}$, defined as $J_{mn} \equiv \partial F_m/\partial L_n$, has

$$\det \underline{J}(\mathbf{L}; \lambda_{min}) = 0. \tag{6}$$

Combining Eq.(6) with Eqs.(5a-5d) gives a total of 5 root equations for the approximate critical coupling and associated limit-cycle.

In practice, if we consider symmetric collisions or asymmetry in the α's only (as we do in the remainder), the above results simplify. For example, in the case of symmetric collisions the relevant branch of stable limit cycles have $R_1 = R_2$, $\gamma = \pi$, and $\omega = \sqrt{\alpha/\beta}/R_1$. Moreover, the symmetric critical coupling predicts a scaling collapse:

$$\lambda_{min} N\beta/2\alpha = 1 \Big/ R_1^2 \int_0^{2\pi}\int_0^R \frac{2rdrd\phi}{\pi R^2} \cdot \frac{\frac{C}{l}e^{-d/l} - e^{-d}}{d} \cdot$$
$$\left[1 - \frac{(2R_1 - r\cos\phi)^2}{d^2} - \frac{(2R_1 - r\cos\phi)^2}{d} \cdot \frac{\frac{C}{l^2}e^{-d/l} - e^{-d}}{\frac{C}{l}e^{-d/l} - e^{-d}}\right]. \tag{7}$$

where the left hand side is a function of the pairwise-interaction parameters only. In addition, $\lambda_{min} \sim v^2$, where v is the speed of each flock, $\sqrt{\alpha/\beta}$.

Comparisons between the measured λ_{min} from scattering diagrams, e.g., Fig.1(a), and the above predictions from Eq.(6) and Eqs.(5a-5d) are shown in Fig.4. In the left subplot (a), we show results for collisions with symmetric parameters with a large variety of N's and α's. As demonstrated with Eq.(7) our predicted scaling collapse holds. Qualitatively, the critical coupling increases monotonically with C, implying that the stronger the strength of repulsion, the larger the coupling needs to be in order for colliding swarms to form a MS. Also, note that our mean-field predictions are fairly robust to heterogeneities in the numbers in each flock, particularly for smaller values of $C/l - 1$; predictions remain accurate for number heterogeneity as large as 20%.

On the other hand, in Fig.4(b) we compare the measured λ_{min} and predictions as a function of asymmetry in the self-propulsion force constant for different N's. The first swarm has $\alpha^{(1)} = 1$, while $\alpha^{(2)}$ is varied. Contrary to the symmetric case the scaling collapse disappears, apart from N. Moreover, the branch of stable limit cycles with equal radii $R_1 = R_2$ disappears in a cusp bifurcation (the solid-black line in in Fig.4(b) vanishes for $\alpha^{(2)} \gtrsim 1.5$). Above the cusp point, the upper branch of SNs corresponds to stable limit cycles where $R_1 < R_2$ and $\gamma = -\pi/2$, shown with a dashed-black line. Interestingly, we can see that for larger values of $\alpha^{(2)} - \alpha^{(1)}$ the critical coupling is nearly linear in the difference, meaning that if one flock doubles its speed, then the coupling needed to form a MS is expected to quadruple – again, a consequence of the flock speed equalling $\sqrt{\alpha/\beta}$. Finally, note that as in (a), predictions remain accurate for a significant range of differences in the numbers in each flock.
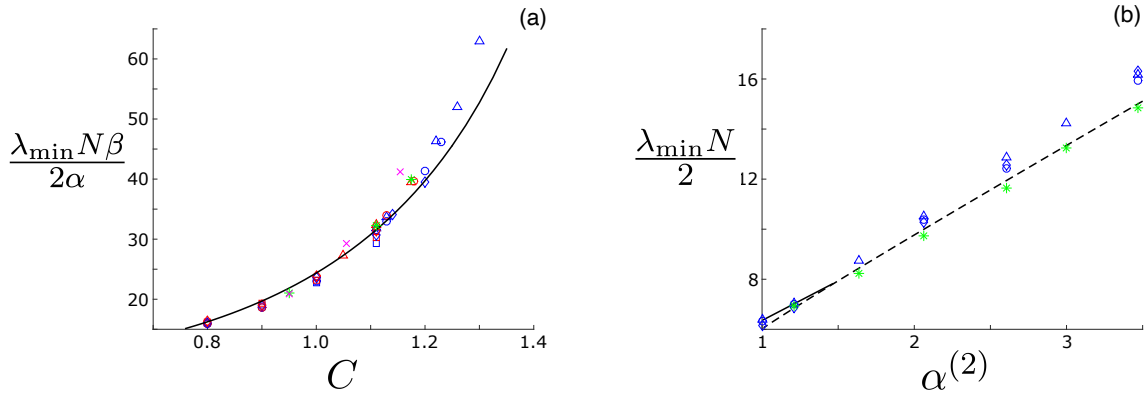
Figure 4. Critical coupling for forming milling states upon collision. (a) Symmetric parameter collisions for $\alpha = 1$ (blue) and $\alpha = 2$ (red): $N = 10$ (squares), $N = 20$ (diamonds), $N = 40$ (circles), and $N = 100$ (triangles). Green stars denote $\alpha = 1$ and magenta x's denote $\alpha = 2$, when 40 agents collide with 60. (b) Asymmetric collisions for $C = 10/9$ in which $\alpha^{(1)} = 1$. Blue points indicate equal numbers in each flock: $N = 20$ (diamonds), $N = 40$ (circles), and $N = 100$ (triangles). Green stars denote collisions between 40 agents with $\alpha^{(1)} = 1$ and 60 agents with $\alpha^{(2)}$. Solid and dashed lines indicate theoretical predictions for (a) and (b), respectively from solving Eqs.(5a-5d) and Eq.(6). Other swarm parameters are $\beta = 5$ and $l = 0.75$.

3 Conclusions

To summarize, in this work we studied the collision of two swarms with nonlinear interactions, and focused in particular on predicting when such swarms would combine to form a mill. Unlike the full scattering diagram, which depends on whether or not a particular set of initial conditions falls within the high-dimensional basin-of-attraction for milling (a hard problem in general), we concentrated on predicting the minimum coupling needed to sustain a mill for near head-on collisions. By noticing that colliding swarms, which eventually form a mill, initially rotate around a common center with an approximately constant density, we were able to transform the question of a critical coupling into determining the stability of limit-cycle states within a mean-field approximation. Our bifurcation analysis agreed well with many-agent simulations. Future robotics experiments, similar to [48, 49], will be used to further test and verify our analysis.

Though our analysis dealt directly with soft-core interacting swarms, the basic approach could be easily extended to a broader range of models, as long as the nonlinear forces between agents have a finite range. A straightforward way to improve the accuracy of our analysis would be to move beyond the uniform-density assumption, and replace it with an exact steady-state density for flocking states with general interactions. Another next-step for improvement would be to include the density dynamics directly, which may provide further quantitative insights for controlling swarm collisions, including in other setups such as flocks-vs-mills. On the other hand, at a broader level our approach assumed that all agents are subject to the same basic physics, irrespective of the swarm

to which they are apart. This is a very classical and standard assumption, and means that when agents from different swarms enter each other's sensing range, they still execute the same low-level controllers. The assumption makes sense if the swarms are composed of similar agents, e.g., birds, insects, etc. From a robotics perspective, one could even think of scenarios where two swarms execute the controlled behavior in order to "scope out" the other swarm. However, one would expect this initial phase to be limited. Therefore, an interesting avenue for future work would be to study how disparate inter swarm interactions affect swarm-on-swarm behavior. Nonetheless, this work takes an important step towards understanding and analyzing the basic collision dynamics of self-propelled swarms with nonlinear interactions, and provides new methods by which they can be quantitatively predicted.

4   Acknowledgments

5   References

[1] Guy Theraulaz, Eric Bonabeau, Stamatios C. Nicolis, Ricard V. Solé, Vincent Fourcassié, Stéphane Blanco, Richard Fournier, Jean-Louis Joly, Pau Fernández, Anne Grimal, Patrice Dalle, and Jean-Louis Deneubourg. Spatial patterns in ant colonies. *Proceedings of the National Academy of Sciences*, 99(15):9645–9649, 2002.

[2] Chad M. Topaz, Maria R. D'Orsogna, Leah Edelstein-Keshet, and Andrew J. Bernoff. Locust dynamics: Behavioral phase change and swarming. *PLoS Comput. Biol.*, 8(8):1–11, 08 2012.

[3] A.A. Polezhaev, R.A. Pashkov, A. I. Lobanov, and I. B. Petrov. *Int. J. Dev. Bio.*, 50:309, 2006.

[4] Jinchao Li and Ali H. Sayed. Modeling bee swarming behavior through diffusion adaptation with asymmetric information sharing. *EURASIP Journal on Advances in Signal Processing*, 2012(1):18, Jan 2012.

[5] George F. Young, Luca Scardovi, Andrea Cavagna, Irene Giardina, and Naomi E. Leonard. Starling flock networks manage uncertainty in consensus at low cost. *PLOS Computational Biology*, 9(1):1–7, 01 2013.

[6] M. Ballerini, N. Cabibbo, R. Candelier, A. Cavagna, E. Cisbani, I. Giardina, V. Lecomte, A. Orlandi, G. Parisi, A. Procaccini, M. Viale, and V. Zdravkovic. Interaction ruling animal collective behavior depends on topological rather than metric distance: Evidence from a field study. *Proceedings of the National Academy of Sciences*, 105(4):1232–1237, 2008.

[7] Andrea Cavagna, Lorenzo Del Castello, Irene Giardina, Tomas Grigera, Asja Jelic, Stefania Melillo, Thierry Mora, Leonardo Parisi, Edmondo Silvestri, Massimiliano Viale, and Aleksandra M. Walczak. Flocking and turning: a new model for self-organized collective motion. *Journal of Statistical Physics*, 158(3):601–627, Feb 2015.

[8] Kolbjà̧rn Tunstrà̧m, Yael Katz, Christos C. Ioannou, Cristià¡n Huepe, Matthew J. Lutz, and Iain D. Couzin. Collective states, multistability and transitional behavior in schooling fish. *PLOS Computational Biology*, 9(2):1–11, 02 2013.

[9] Daniel S Calovi, Ugo Lopez, Sandrine Ngo, Clément Sire, Hugues Chaté, and Guy Theraulaz. Swarming, schooling, milling: phase diagram of a data-driven fish school model. *New Journal of Physics*, 16(1):015026, jan 2014.

[10] Kevin Rio and William H. Warren. The visual coupling between neighbors in real and virtual crowds. *Transportation Research Procedia*, 2:132 – 140, 2014. The Conference on Pedestrian and Evacuation Dynamics 2014 (PED 2014), 22-24 October 2014, Delft, The Netherlands.

[11] Frank Cichos, Kristian Gustavsson, Bernhard Mehlig, and Giovanni Volpe. Machine learning for active matter. *Nature Machine Intelligence*, 2(2):94–103, 2020.

[12] T. Vicsek and A. Zafeiris. *Phys. Rep.*, 517:71, 2012.

[13] M. C Marchetti, J. F Joanny, S. Ramaswamy, T. B Liverpool, J. Prost, M. Rao, and R. A Simha. *Rev. Mod. Phys.*, 85:1143, 2013.

[14] M. Aldana, V. Dossetti, C. Huepe, V. M Kenkre, and H. Larralde. *Phys. Rev. Letts.*, 98:095702, 2007.

[15] A. Solon, Y. Fily, A. Baskaran, M. E. Cates, Y. Kafri, M. Kardar, and J. Tailleur. Pressure is not a state function for generic activeÊfluids. *Nature Phys.*, 11:673, 2015.

[16] Étienne Fodor, Cesare Nardini, Michael E. Cates, Julien Tailleur, Paolo Visco, and Frédéric van Wijland. How far from equilibrium is active matter? *Phys. Rev. Lett.*, 117:038103, Jul 2016.

[17] Francis G. Woodhouse, Henrik Ronellenfitsch, and Jörn Dunkel. Autonomous actuation of zero modes in mechanical networks far from equilibrium. *Phys. Rev. Lett.*, 121:178001, Oct 2018.

[18] E. Woillez, Y. Zhao, Y. Kafri, V. Lecomte, and J. Tailleur. Activated escape of a self-propelled particle from a metastable state. *Phys. Rev. Lett.*, 122:258001, Jun 2019.

[19] J. P. Desai, J. P. Ostrowski, and V. Kumar. Modeling and control of formations of nonholonomic mobile robots. In *IEEE Transactions on Robotics and Automation*, volume 17(6), pages 905–908, 2001.

[20] A. Jadbabaie, Jie Lin, and A. S. Morse. Coordination of groups of mobile autonomous agents using nearest neighbor rules. *IEEE Transactions on Automatic Control*, 48(6):988–1001, June 2003.

[21] H. G. Tanner, A. Jadbabaie, and G. J. Pappas. Stable flocking of mobile agents part ii: dynamic topology. In *42nd IEEE International Conference on Decision and Control (IEEE Cat. No.03CH37475)*, volume 2, pages 2016–2021 Vol.2, Dec 2003.

[22] H. G. Tanner, A. Jadbabaie, and G. J. Pappas. Stable flocking of mobile agents, part i: fixed topology. In *42nd IEEE International Conference on Decision and Control (IEEE Cat. No.03CH37475)*, volume 2, pages 2010–2015 Vol.2, Dec 2003.

[23] V. Gazi. Swarm aggregations using artificial potentials and sliding-mode control. *IEEE Transactions on Robotics*, 21(6):1208–1214, Dec 2005.

[24] H. G. Tanner, A. Jadbabaie, and G. J. Pappas. Flocking in fixed and switching networks. *IEEE Transactions on Automatic Control*, 52(5):863–868, May 2007.

[25] R. Siegwart, I.R. Nourbakhsh, and D. Scaramuzza. *Autonomous Mobile Robots*. MIT Press, London, 2011.

[26] I. D. Miller, F. Cladera, A. Cowley, S. S. Shivakumar, E. S. Lee, L. Jarin-Lipschitz, A. Bhat, N. Rodrigues, A. Zhou, A. Cohen, A. Kulkarni, J. Laney, C. J. Taylor, and V. Kumar. Mine tunnel exploration using multiple quadrupedal robots. *IEEE Robotics and Automation Letters*, 5(2):2840–2847, 2020.

[27] D. Pickem, P. Glotfelter, L. Wang, M. Mote, A. Ames, E. Feron, and M. Egerstedt. The robotarium: A remotely accessible swarm robotics research testbed. In *2017 IEEE International Conference on Robotics and Automation (ICRA)*, pages 1699–1706, 2017.

[28] E. Kagan, N. Shvalb, and I. Ben-Gal. *Autonomous Mobile Robots and Multi-Robot Systems: Motion-Planning, Communication, and Swarming*. Wiley, Hoboken, NJ, 2020.

[29] Ragesh K. Ramachandran, Karthik Elamvazhuthi, and Spring Berman. *An Optimal Control Approach to Mapping GPS-Denied Environments Using a Stochastic Robotic Swarm*, pages 477–493. Springer International Publishing, Cham, 2018.

[30] H. Li, C. Feng, H. Ehrhard, Y. Shen, B. Cobos, F. Zhang, K. Elamvazhuthi, S. Berman, M. Haberland, and A. L. Bertozzi. Decentralized stochastic control of robotic swarm density: Theory, simulation, and experiment. In *2017 IEEE/RSJ International Conference on Intelligent Robots and Systems (IROS)*, pages 4341–4347, Sep. 2017.

[31] S. Berman, A. Halasz, V. Kumar, and S. Pratt. Bio-inspired group behaviors for the deployment of a swarm of robots to multiple destinations. In *Proceedings 2007 IEEE International Conference on Robotics and Automation*, pages 2318–2323, April 2007.

[32] M. Ani Hsieh, Ádám Halász, Spring Berman, and Vijay Kumar. Biologically inspired redistribution of a swarm of robots among multiple sites. *Swarm Intelligence*, 2(2):121–141, Dec 2008.

[33] Wai Kit Wong, Shujin Ye, Hai Liu, and Yue Wang. Effective Mobile Target Searching Using Robots. *Mobile Networks and Applications*, 2020.

[34] Hoam Chung, Songhwai Oh, David Hyunchul Shim, and S. Shankar Sastry. Toward robotic sensor webs: Algorithms, systems, and experiments. *Proceedings of the IEEE*, 99(9):1562–1586, 2011.

[35] Ulf Witkowski and Mohamed El Habbal. Ad-hoc network communication infrastructure for multi-robot systems in disaster scenarios. *6th Framework program of European Union*.

[36] M. Rubenstein, C. Ahler, and R. Nagpal. Kilobot: A low cost scalable robot system for collective behaviors. In *2012 IEEE International Conference on Robotics and Automation*, pages 3293–3298, 2012.

[37] K. Petersen, R. Nagpal, and J. Werfel. Termes: An autonomous robotic system for three-dimensional collective construction. In *Conference: Robotics: Science and Systems VII*, pages 3293–3298, 2012.

[38] Guillaume Sartoretti and Max-Olivier Hongler. Interacting brownian swarms: Some analytical results. *Entropy*, 18(1), 2016.

[39] H. Levine, W. J. Rappel, and I. Cohen. *Phys. Rev. E*, 63:017101, 2000.

[40] U. Erdmann, W. Ebeling, and A. S. Mikhailov. *Phys. Rev. E*, 71:051904, 2005.

[41] E. Minguzzi. Rayleigh's dissipation function at work. *European Journal of Physics*, 36:035014, 2015.

[42] M. R D'Orsogna, Y. L Chuang, A. L Bertozzi, and L. S Chayes. *Phys. Rev. Lett.*, 96:104302, 2006.

[43] L. Mier y Teran-Romero, E. Forgoston, and I. B. Schwartz. Coherent pattern prediction in swarms of delay-coupled agents. *IEEE Transactions on Robotics*, 28(5):1034–1044, Oct 2012.

[44] Yuxin Chen and Theodore Kolokolnikov. A minimal model of predator-swarm interactions. *Journal of the Royal Society, Interface / the Royal Society*, 11(94):20131208, may 2014.

[45] Dieter Armbruster, Stephan Martin, and Andrea Thatcher. Elastic and inelastic collisions of swarms. *Physica D: Nonlinear Phenomena*, 344:45 – 57, 2017.

[46] Carl Kolon and Ira B Schwartz. The dynamics of interacting swarms. *arXiv preprint arXiv:1803.08817*, 2018.

[47] Jason Hindes, Victoria Edwards, Sayomi Kamimoto, George Stantchev, and Ira B. Schwartz. Stability of milling patterns in self-propelled swarms on surfaces. *Physical Review E*, 102:022212, 2020.

[48] Klementyna Szwaykowska, Ira B Schwartz, Luis Mier-y-Teran Romero, Christoffer R Heckman, Dan Mox, and M Ani Hsieh. Collective motion patterns of swarms with delay coupling: Theory and experiment. *Physical Review E*, 93(3):032307, 2016.

[49] Victoria Edwards, Philip deZonia, M. Ani Hsieh, Jason Hindes, Ioana Triandaf, and Ira B. Schwartz. Delay induced swarm pattern bifurcations in mixed reality experiments. *Chaos*, 30:073126, 2020.

[50] Jason Hindes, Victoria Edwards, Sayomi Kamimoto, Ioana Triandaf, and Ira B Schwartz. Unstable modes and bistability in delay-coupled swarms. *Physical Review E*, 101(4):042202, 2020.

[51] A. Bernoff and C.M Topaz. *SIAM Journal of Applied Dynamical Systems*, 10:212, 2011.

[52] J.A. Carrillo, Y. Huang, and S. Martin. Nonlinear stability of flock solutions in second-order swarming models. *Nonlinear Analysis: Real World Applications*, 17:332 – 343, 2014.